Vanadium centers in ZnTe crystals. I. Optical properties

P. Peka, M. U. Lehr,* and H.-J. Schulz
Fritz-Haber-Institut der Max-Planck-Gesellschaft, Faradayweg 4-6, D-14195 Berlin, Germany

U. W. Pohl
Institut für Festkörperphysik, Technische Universität Berlin, Hardenbergstrasse 36, D-10623 Berlin, Germany

J. Kreissl and K. Irmscher
Arbeitsgruppe Elektron-Paramagnetische Resonanz am Institut für Festkörperphysik, Technische Universität Berlin, Haus 11.4, Rudower Chaussee 5, D-12484 Berlin, Germany

(Received 24 July 1995)

In ZnTe:V bulk crystals with nominal vanadium concentrations between 1000 and 7000 ppm three vanadium-ion states V^+, V^{2+}, and V^{3+} were found in low-temperature optical measurements. No-phonon lines of the internal emissions were detected for the ${}^5E(D)\rightarrow{}^5T_2(D)$ transition of $V^+(d^4)$ at 3401 cm^{-1} (0.422 eV), for ${}^4T_2(F)\rightarrow{}^4T_1(F)$ of $V^{2+}(d^3)$ at 4056 cm^{-1} (0.503 eV), and for ${}^3T_2(F)\rightarrow{}^3A_2(F)$ of $V^{3+}(d^2)$ at 4726 cm^{-1} (0.586 eV). The energies of the internal transitions are reduced with respect to the corresponding transitions in ZnS:V and ZnSe:V. The respective excitation spectra display, in addition to broad charge-transfer bands, higher excited levels of the individual charge states. Crystal-field calculations of the detected transition energies based on the Tanabe-Sugano scheme are presented. With the help of sensitization experiments, a one-electron model is designed, in which the donor level (V^{2+}/V^{3+}) is situated 12 500 cm^{-1} (1.55 eV) below the conduction-band edge and the acceptor level (V^{2+}/V^{+}) 9400 cm^{-1} (1.17 eV) above the valence-band edge. The dynamical behavior of the three infrared luminescence bands was measured. Decay time constants of 43 μs (V^+), 120 μs (V^{2+}), and 420 μs (V^{3+}) were found. Electron-paramagnetic-resonance (EPR) results measured on the same samples are presented in an accompanying paper and confirm the optical detection of isolated substitutional $V^{2+}(d^3)$ and $V^{3+}(d^2)$ ions. Relations between the EPR and optical results are discussed.

I. INTRODUCTION

Optical properties of vanadium have been studied for a long time in various II-VI compound semiconductors. Up to now, however, almost no information was available on luminescence properties of vanadium-activated ZnTe. During the past years, this material has attracted increasing interest stimulated by possible applications of the photorefractive properties in the wavelength region 0.6–1.3 μm.[1]

In CdTe, vanadium creates a deep donor level and increases the resistivity, due to compensation of intrinsic defects, which act as acceptors.[2–5] A similar compensation is found in titatium-doped (Cd,Zn)Te (Ref. 6) as well. A comparable situation might be expected in ZnTe, which also tends to be intrinsically p type. On the other hand, an amphoteric behavior of the substitutional V impurity is found in ZnSe:V (Ref. 7) and ZnS:V (Ref. 8). The vanadium ions can analogously be assumed to replace cations here, so that the optical properties will be determined by V_{Zn} centers, which will have a T_d environment in a first approximation. Existence of both a donor and an acceptor state is evidenced by $V^+(d^4)$ spectra appearing in addition to internal transitions of $V^{2+}(d^3)$ and $V^{3+}(a^2)$. According to the Langer-Heinrich model,[9] the conduction-band (CB) minimum of ZnTe is placed about 3800 cm^{-1} above that of the ZnSe, so that there is enough space for the $(0/-)$-acceptor level of vanadium within the ZnTe gap. Therefore, the $V^+(d^4)$ in ZnTe should be detectable.

The only mention of luminescence of ZnTe:V so far is not sustained by a spectrum.[1] Two strong low-temperature photoluminescence bands near 8600 cm^{-1} (1.065 eV) with 690 cm^{-1} [full width at half maximum (FWHM)] and near 12 900 cm^{-1} (1.60 eV) with 2000 cm^{-1} FWHM accompanied by a weak band near 6650 cm^{-1} (0.825 eV) with 1100-cm^{-1} FWHM are reported. In the present work, a detailed analysis of optical transitions of V in ZnTe is advanced. An assignment of the observed luminescence bands and corresponding excitation spectra to V transitions is based on crystal-fields calculations. Additional sensitization spectra reflect the charge-transfer properties of the vanadium impurity.

II. EXPERIMENTAL RESULTS

ZnTe:V bulk crystals were grown from a stochiometric melt by the vertical high-pressure Bridgman method. Doping was performed during growth by adding elemental vanadium. The nominal concentrations in the studied samples were 1000, 1500, and 7000 ppm.

The optical measurements were conducted at low temperature with samples mounted in a He immersion cryostat. An Ar^+ laser (emission measurements) or Xe lamps (excitation and sensitization measurements) were used as excitation sources. The technique of sensitization spectroscopy is a special kind of excitation spectroscopy, using two light sources, a modulated and an unmodulated one. One of them is kept at a fixed wavelength, while the other one is scanned. The difference between sensitization spectroscopy and excitation

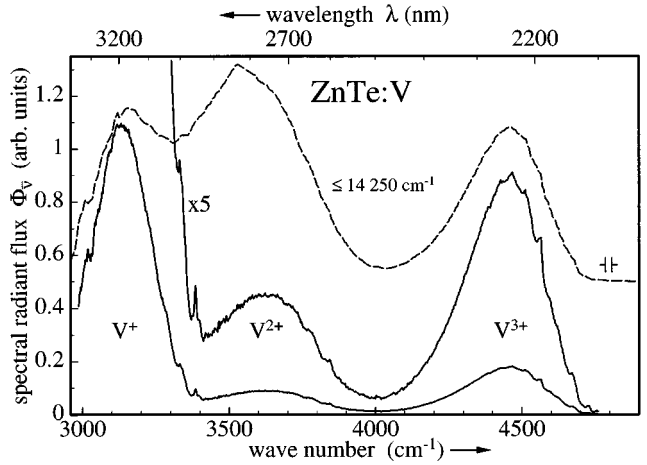

FIG. 1. Photoluminescence spectra of ZnTe:V at $T=4.2$ K, under Ar^+ laser excitation at 528.7 nm (18 915 cm^{-1}). The center curve is five times enlarged to show the fine structures of V^{3+}. The dashed line represents the luminescence under additional unmodulated irradiation at $\bar{\nu} \leqslant 14\,250$ cm^{-1}. This spectrum is shifted upwards by 0.5 arb. units. The bands are assigned to the lowest-energy transitions of the +, 2+, and to 3+ charge states of vanadium ions (*from left to right*).

spectroscopy with additional irradiation is that in the former case the unmodulated excitation wavelength is varied. Thus, the beneficial or deteriorating effect of pumping at different wavelengths, i.e., population or depopulation of certain states, on the observed excitation-emission channel is monitored. The experimental setup for the sensitization experiments is also described in Ref. 10.

For the study of its dynamical behavior, the luminescence was excited by a Q-switched Nd:YAG laser at 9400 cm^{-1} or at 18 800 cm^{-1} and detected in the same energy regions as in the measurements of excitation spectra. A liquid-nitrogen-cooled InSb detector with 1-MHz bandwidth, a transient recorder, and an averaging computer were used for signal amplification and data processing. Under both these excitation energies, the results for the three internal V emissions were the same. The measurements delivered in a good approximation exponential curves from which time constants were obtained in half-logarithmic plots.

A. Emission spectra

In vanadium-activated ZnTe, three luminescence bands appearing simultaneously were detected in the range between 3000 and 5000 cm^{-1} under band-to-band excitation. The weakly structured bands are centered near 3130, 3580, and 4450 cm^{-1}, cf Fig. 1. Their intensity ratios were found to depend on the individual sample and on the energy of a possible auxiliary excitation. The overall picture resembles the luminescence of vanadium-activated ZnS (Ref. 8) and ZnSe (Ref. 7). In these host crystals, doping with vanadium leads to three structured emission bands originating from luminescent internal relaxations of the three charge states V^+, V^{2+}, and V^{3+}. Based on the apparent similarities, the three emission bands of ZnTe:V are likewise attributed to the same crystal-field transitions. In the transition energies of all three bands, a decrease by a factor of 0.9 ± 0.05 is observed on going from ZnS over ZnSe to ZnTe. Such a chemical trend is well-known from crystal-field transitions of other TM impurities. In the following, this intuitive assignment will be supported by further details of the optical properties [e.g., for $V^{3+}(d^2)$ a reduced TO phonon in the emission band, the three excitation spectra, time constants] and crystal-field calculations.

The luminescence band lowest in energy shows a no-phonon doublet with lines at 3388 and 3401 cm^{-1}. Since no thermalization was found, the corresponding splitting is attributed to the ground state. The fine structure exhibits features similar to those observed for $V^+(d^4)$ ions in ZnS:V and ZnSe:V,[11] and the trend is confirmed for ZnTe:V. Due to heavier ligand atoms and thus smaller lattice-phonon energies, the no-phonon lines (NPL) become successively weaker and less pronounced in ZnTe. A threefold fine splitting observed in ZnS:V is already quenched to a twofold splitting in ZnSe:V and to a single line at 3401 cm^{-1} in ZnTe. The line at 3388 cm^{-1} corresponds to a NPL structure in ZnS, there in a distance of 38 cm^{-1} and in ZnSe of 23 cm^{-1} from the respective high-energy NPL.[12] Structures at 3336 and 3286 cm^{-1} are assigned to a TA phonon and a quasilocal mode, respectively. The luminescence is decaying exponentially after pulse excitation. The mean life time was found to be $\tau=(43\pm2)$ μs.

The luminescence band centered near 3580 cm^{-1} shows only a very weak no-phonon structure at 4056 cm^{-1}. The corresponding $V^{2+}(d^3)$ emissions in ZnS:V and ZnSe:V exhibit two and six no-phonon lines (NPL), respectively. Weak phonon satellites of TA(X) modes, a quasilocal vibration, LA(X) and LO(Γ) modes are recognized at 4005, 3957, 3911, and 3844 cm^{-1}, respectively. The assignment of this luminescence to a ${}^4T_2(F)\rightarrow{}^4T_1(F)$ transition of V^{2+} is predominantly supported by its excitation features described in Sec. II B. After pulse excitation a monoexponential decay is found, described by a lifetime $\tau=(120\pm10)$ μs.

The emission band centered at 4450 cm^{-1} shows more pronounced structures than the two emissions of lower energy. A no-phonon line is detected at 4726 cm^{-1}, a pronounced TO satellite at 4563 cm^{-1}. This slightly reduced gap mode is a characteristic feature of the V^{3+} luminescence in various host crystals: ZnS:V (Ref. 8), ZnSe:V (Ref. 7), GaAs and GaP (Refs. 13 and 14) and InP (Refs. 15 and 16). A rise of the temperature does not change the relative intensities of the lines in the NPL region. Wide-range excitation increases the coupling to lattice vibrations so that the NPL is no more resolvable. This ${}^3T_2(F)\rightarrow{}^3A_2(F)$ emission of $V^{3+}(d^2)$ which is symmetry forbidden in T_d, decays exponentially with $\tau=(420\pm20)$ μs.

The ground state ${}^3A_2(F)$ of a d^2 configuration does not split under the influence of spin-orbit coupling in cubic symmetry, therefore, the three further weak lines in the no-phonon range, namely, at 4837, 4785, and 4760 cm^{-1}, do not show a close connection to the $V^{3+}(d^2)$ emission of isolated vanadium ions. They are assumed to be related to a trigonal center detected by EPR (see paper II) consisting of a defect X_{Te} associated with $V_{Zn}{}^{3+}$.

Besides these emission bands of the three vanadium ionization states in the low-energy region, two further luminescence bands were detected at 6000 and 8600 cm^{-1}, with a FWHM of 700 cm^{-1}. They are probably identical with those

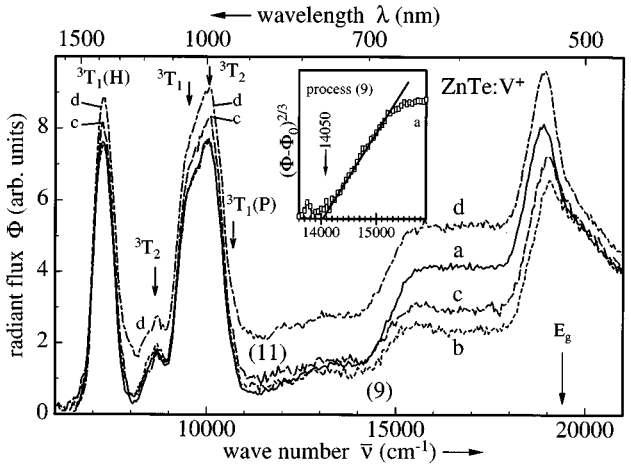

FIG. 2. Excitation spectrum of the ${}^5E(D)\rightarrow{}^5T_2(D)$ luminescence of $V^+(d^4)$ at $T=4.2$ K. Detected emission range: $\overline{\nu}=2900-3300\ \mathrm{cm}^{-1}$. Curve (a) is measured without additional excitation. Additional unmodulated irradiations during recording of curve (b): $\overline{\nu}=9800-10\ 200\ \mathrm{cm}^{-1}$; curve (c): $\overline{\nu}=12\ 900-13\ 800\ \mathrm{cm}^{-1}$; and curve (d): $17\ 400-19\ 000\ \mathrm{cm}^{-1}$. All other conditions of experiment were the same. In the inset, the $\frac{2}{3}$ power fit of the CT band (9) is displayed.

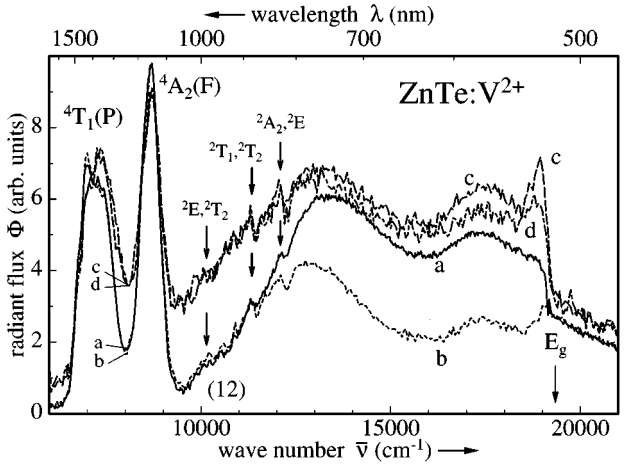

FIG. 3. Excitation spectrum of the ${}^4T_2(F)\rightarrow{}^4T_1(F)$ luminescence of ZnTe:$V^{2+}(d^3)$ at $T=4.2$ K. Detected emission range: $\overline{\nu}=3330-3950\ \mathrm{cm}^{-1}$. Curve (a) is measured without additional irradiation, while additional unmodulated irradiations during detection of curves (b), (c), and (d) are the same as in Fig. 2 [i.e., at (b): 10 000; (c): 13 300; and (d): $18\ 200\ \mathrm{cm}^{-1}$].

mentioned in the text of Ref. 1. We observe a distinct NPL in emission and a weak one in the absorption at $6645\ \mathrm{cm}^{-1}$ in the first case, and a very weak NPL at $9218\ \mathrm{cm}^{-1}$ in emission in the second case.

In the sidebands of almost all the described luminescence bands (with the exception of the highest-energy band around $8600\ \mathrm{cm}^{-1}$), a phonon peak with an energy of about $100\ \mathrm{cm}^{-1}$ can be resolved. This energy range corresponds to the LA phonon wing of ZnTe.[17] These phonon peaks are probably caused by quasilocal modes related to vanadium.

B. Excitation spectra

The three V emission bands described above exhibit different pronounced excitation bands. Selective excitation spectra were recorded using three broad band-pass ranges (Figs. 2, 3, and 4). The classifications of the excitation peaks of the internal transitions are listed in Table I. For comparison, the centers of gravity of the corresponding bands of vanadium in ZnSe (Refs. 7 and 11) are also listed in this table. The maxima (centers of gravity) of the excitation bands of the internal transitions are marked in the spectra by arrows. In the excitation and sensitization spectra, the starting points of the charge-transfer (CT) processes are additionally marked with numbers in parentheses. The CT processes and the three vanadium emissions are listed in Table II and are described with the help of a one-electron model (Fig. 5) (compare, e.g., Ref. 10). The model comprises the ground and first excited states of the three ionization states of vanadium; thus, six columns result, each consisting of valence-band (VB) maximum, e level, t_2 level, conduction-band (CB) minimum, and electrons on these levels symbolized by small arrows. Each column corresponds to one weak-field state, in the figure given in the second row from bottom. Charge-transfer processes are described by arrows connecting the initial and the terminal state of a transition. The number of electrons is changed only on touched levels, and just one electron can be moved in a process described by one arrow. The vertical component of the CT arrow represents the threshold energy of the transition. The higher excited states are not included in the model, because it is assumed that they do not play an important role in charge-transfer processes, for reasons of fast relaxation to the lower states.

The $V^+(d^4)$ excitation spectrum (Fig. 2) shows two strong bands, a narrower one at $7250\ \mathrm{cm}^{-1}$ and a broad one at $9500-10\ 000\ \mathrm{cm}^{-1}$. Between these two bands, at $8600\ \mathrm{cm}^{-1}$, a smaller but well-resolved band can be recognized. The excitation structures below $11\ 000\ \mathrm{cm}^{-1}$ can be readily as-

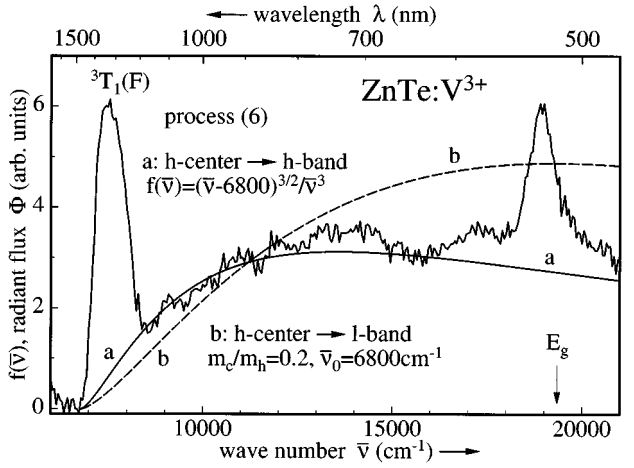

FIG. 4. Excitation spectrum of the ${}^3T_2(F)\rightarrow{}^3A_2(F)$ luminescence of ZnTe:$V^{3+}(d^2)$ at $T=4.2$ K. Detected emission range: $\overline{\nu}=4350-4760\ \mathrm{cm}^{-1}$. The lines (a) and (b) exhibit the theoretical fits of the charge-transfer band (6). Approximation curve (a) represents the transition from the h center to the h valence band and (b) the transition from the h center to the l valence band (see text and Ref. 19).

TABLE I. Compilation of the energies of the internal transitions of the $V^+(d^4)$, $V^{2+}(d^3)$, and $V^{3+}(d^2)$ ions in ZnTe, compared to the respective transitions in ZnSe. The energies of the transitions in ZnTe are taken from the excitation spectra (Figs. 2–4). The energies marked with * are deduced from the emission spectra in Fig. 1 and from the NPL (see text). The ZnSe:V^+ data are taken from Ref. 11, the ZnSe:V^{2+}, and ZnSe:V^{3+} data from Ref. 7. All values are given in cm^{-1}. The data in parentheses represent very weak bands, while the strongest bands are typed in bold letters.

Ion/ ground state	Rising point	Absorption band (center of gravity) ZnTe	Identification	Absorption band (center of gravity) ZnSe
$V^+(d^4)/^5T_2(D)$	3410=NPL	3650*	$^5E(D)$	3840
	6700	**7250**	$^3T_1(H)$	**7830**
	8200	8600	$^3T_2(H)$	8800
	9000	**9500**	$^3T_1(H)$	**10 250**
		10 000	$^3T_2(F)$	**10 900**
		10 750	$^3T_1(P)$	12 000
$V^{2+}(d^3)/^4T_1(F)$	4056=NPL	4450*	$^4T_2(F)$	5110
			$^2T_1(H)$	(6770)
	6550	**7200**	$^4T_1(P)$	**8350**
	8150	**8680**	$^4A_2(F)$	**10 220**
		(10 100)	$^2E(H),^2T_2(D)$	11 930
		(11 300)	$^2T_1(H),^2T_2(F)$	13 540
		(12 100)	$^2A_2(F),^2E(D)$	15 000
			$^2T_1(F)$	(16 200)
$V^{3+}(d^2)/^3A_2(F)$	4726=NPL	5000*	$^3T_2(F)$	5760
	6900	**7500**	$^3T_1(F)$	**8890**
			$^3T_1(P)$	**13 350**

signed to transitions into triplet states of V^+. The assignments denoted in Fig. 2 are discussed in Sec. II C. Transition energies and corresponding classifications are summarized in Table I. Although the internal transitions dominating the V^+ excitation spectra are spin forbidden, the strongest of these are as intensive as the near-gap peak. This spectrum is similar to that of ZnSe:V^+ up to 12 000 cm^{-1}, where in ZnSe a strong charge-transfer process starts.[11] In ZnTe, a weaker one commences at 11 000 cm^{-1} as well, assigned to process (11). In addition, a quite strong CT process (No. 9) rises steeply at 14 050 cm^{-1} (for the threshold compare the inset of Fig. 2). Together with the simple excitation spectrum of ZnTe:V^+ (curve *a*), excitation spectra recorded under an auxiliary unmodulated irradiation are displayed, otherwise measured under the same conditions (curves *b*, *c*, and *d*). While additional light at 10 000 cm^{-1} quenches the excitability above 14 000 cm^{-1} (curve *b*), near-gap pump light stimulates the whole spectrum (curve *d*).

In Fig. 3, the excitation spectrum of the $V^{2+}(d^3)$ emission is presented together with three more curves detected under various additional excitations. The spectrum in the low-energy range ($\bar{\nu} \leqslant 10\,000$ cm^{-1}) resembles its equivalent in ZnSe.[7] The two dominating peaks have almost the same shape and are also attributed to the same spin-allowed transitions to quartet levels (see Table I). As with ZnSe:V,[7] the splitting of 400 cm^{-1} observed in the band denoted $^4T_1(P)$ is explained by Jahn-Teller interaction; it is 5% smaller compared to ZnSe. Additional excitation bands (Fig. 3) are evidently covered by a strong CT band (12) and are, therefore, only weakly pronounced. They are ascribed to spin-forbidden transitions (see Table I and Sec. II C). In contrast to the ZnSe:V^{2+} excitation spectrum, another charge-transfer band rises only very slowly, so that these peaks are discernible.

The presence of the spin-forbidden peaks on the rising slope of the CT band (12) complicates an exact determination of the starting point. By means of the usual $\frac{2}{3}$ power law, the threshold is estimated at approximately 9400 cm^{-1}. After reaction (12), the V^{2+} emission is excited through the hole-recapture process (10).

While in the V^{2+} excitation spectrum of ZnSe (Ref. 7), the near-gap band is about ten times stronger than the spin allowed bands $^4T_1(P)$ and $^4A_2(F)$, in ZnTe the near-gap band is missing (Fig. 3 curve *a*). Only under additional illumination, a small maximum appears (curves *b*, *c*, *d*). This situation resembles the excitation spectrum of ZnSe:$Ni^{2+}(d^8)$, where a strong CT band with steep slope also exists and no near-gap peak can be detected (e.g., Ref. 18). In ZnSe:Ni, this band endowed with NP lines at the onset is assigned to the CT process $Ni^{2+}+h\nu \rightarrow (Ni^+,e^+)$, which leads to a bound-exciton state (Ni^{2+},X).[18] Analogously, the present CT band with the rising point at 9400 cm^{-1} is assigned to the acceptor process (12). By additional excitation with 13 300 cm^{-1} (curve *c*) and 18 200 cm^{-1} (curve *d*) the low-energy part of the CT band is lifted up and by linear extrapolation of the rising slope the onset energy can be determined as 7000 cm^{-1} approximately (process 6). In contrast, the two high-energy excitation bands at 13 500 cm^{-1} and 17 500 cm^{-1} become weaker under additional excitation at 10 000 cm^{-1} (curve *b*).

The excitation spectrum of the $V^{3+}(d^2)$ emission in ZnTe (Fig. 4) shows one strong band at 7500 cm^{-1}, reflecting the

TABLE II. Compilation of the CT processes included in the one-electron model along with the internal transitions (2), (3), and (4) (Fig. 5). The low-temperature gap of ZnTe is at 19 300 cm^{-1}. e^-_{CB} and e^+_{VB} label an electron in the conduction band and a hole in the valence band, respectively. The most important energies derived from the experiment are ascribed to the processes Nos. (6), (9), and (12). The table consists of three groups of reactions: internal, V^{3+}/V^{2+} and V^{2+}/V^{+} transitions. The even-numbered CT processes are related to the VB and the odd-numbered processes to the CB.

Process number	Reaction and transition energy	Origin of the numerical data
(2) internal transition	$[V^{3+}]^* \equiv {}^3T_2(F) \leftrightarrow V^{3+} + 4726\ cm^{-1}$	luminescence Fig. 1
(3) internal tr.	$[V^{2+}]^* \equiv {}^4T_2(F) \leftrightarrow V^{2+} + 4056\ cm^{-1}$	luminescence Fig. 1
(4) internal tr.	$[V^{+}]^* \equiv {}^5E(D) \leftrightarrow V^{+} + 3410\ cm^{-1}$	luminescence Fig. 1
(1)	$[V^{3+}]^* + e^-_{CB} \rightarrow [V^{2+}]^* + 13\,100\ cm^{-1}$	not detected (7)–(3)
(5) donor tr.	$V^{2+} + 13\,000\ cm^{-1} \leftrightarrow V^{3+} + e^-_{CB}$	sensitization spectrum of V^{3+} Fig. 9 curve (b); $E_g-(6)$
(6)	$V^{3+} + 6800\ cm^{-1} \leftrightarrow V^{2+} + e^+_{VB}$	excitation spectrum of V^{3+} Fig. 4 and sensitization spectra
(7)	$V^{2+} + 17\,200\ cm^{-1} \leftrightarrow [V^{3+}]^* + e^-_{CB}$	sensitization spectrum of V^{3+} Fig. 9 curve (b)
(8)	$V^{2+} + e^+_{VB} \leftrightarrow [V^{3+}]^* + 2100\ cm^{-1}$	not detected (probably non-radiative), (6)–(2)
(9)	$V^{+} + 14\,050\ cm^{-1} \rightarrow [V^{2+}]^* + e^-_{CB}$	excitation spectrum of V^{+}, Fig. 2
(10)	$V^{+} + e^+_{VB} \rightarrow [V^{2+}]^* + 5500\ cm^{-1}$	not detected (probably non-radiative), (12)–(3)
(11)	$V^{+} + 10\,000\ cm^{-1} \leftrightarrow V^{2+} + e^-_{CB}$	excitation spectrum of V^{+}, (9)–(3)
(12) acceptor tr.	$V^{2+} + 9400\ cm^{-1} \leftrightarrow V^{+} + e^+_{VB}$	excitation spectrum of V^{2+} Fig. 3
(13)	$[V^{2+}]^* + e^-_{CB} \rightarrow [V^{+}]^* + 10\,600\ cm^{-1}$	not detected (9)–(4)

spin-allowed process ${}^3T_1(F) \leftarrow {}^3A_2(F)$ (cf. Sec. II C). At the high-energy side, a very wide band spreads out to the near-gap band, and in the region 16 000–18 000 cm^{-1}, another obscured structure can be assumed. In ZnSe:V^{3+}, a corresponding ${}^3T_1(F)$ excitation band is found[7] accompanied by a second strong excitation via the ${}^3T_1(P)$ level. This excitation transition is missing in ZnTe:V^{3+}. The same situation is found with CdTe:V^{3+} (Ref. 5), where also a CT band starts with a smaller energy than the one expected for the ${}^3T_1(P)$ transition. The reason is given by the distance of the V^{3+}/V^{2+} donor level from the VB. The levels of the excited states lie in a hole model beneath the V^{3+}/V^{2+} donor level, which (in this scheme) represents at the same time the ground state level ${}^3A_2(F)$ of V^{3+}. The ${}^3T_1(P)$ level is below the VB maximum and the excited holes interact easily with the VB continuum and produce V^{2+} (process 6).

In the ZnTe:V absorption spectrum (Fig. 6), a band is detected in the ${}^3T_1(F)$ region, but no ${}^3T_1(P)$ band around 12 000 cm^{-1} is found. The wide CT band in Fig. 4 is assigned to the same CT process (6) as in CdTe:V.[5] The starting point of this CT process is well resolved in many sensitization spectra (e.g., Fig. 10) at 6800 cm^{-1}. After process (6), the V^{3+} emission is excited by the hole-recapture process (8), as in CdTe:V.[5]

Figure 4 also includes a theoretical fit of the broad CT band (6). Among different approximations tested,[19] only the two plotted curves (a and b) are matching the experimental spectrum reasonably. Just these two fits belong to a CT transition from a heavy-hole type (h-type) center to one of the VB's: Curve (a) (Fig. 4) represents a transition to the heavy-hole VB and curve (b) to the light-hole VB. The parameter $m_c/m_h = 0.2$ follows from the fit represented by curve (b). It is in a very good agreement with the published average data $m_c = 0.12 m_0$ for CB and $m_h = 0.6 m_0$ for VB, where m_0 stands for the electron mass.[20] These results support the idea that the $V^{3+}(d^2)$ ion forms a center of the heavy-hole type. This conclusion seems to be reasonable, because the impurity level is found comparatively near to the VB edge. One hole is delivered from a V^{3+} center to the VB by process (6), while the system absorbs the energy of 6800 cm^{-1}.

The excitation spectra of $V^{3+}(d^2)$ change very little under an additional excitation with the light of various energies. By 18 200 cm^{-1} pumping, only the ${}^3T_1(F)$ peak rises and under 10 000 cm^{-1} additional illumination, the 14 500 and 17 500 cm^{-1} bands are stronger. 13 300 cm^{-1} pumping light does not induce any changes.

The excitation spectra of the two higher-energy emission bands (at 6000 cm^{-1} and 8600 cm^{-1}) display a steep slope of

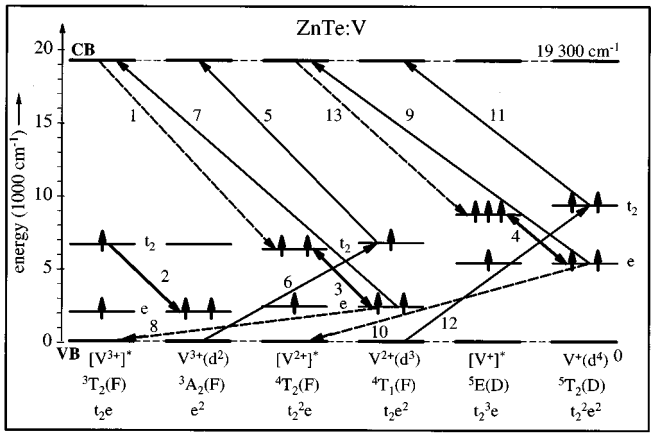

FIG. 5. One-electron model of the $V^{3+}(d^2)$, $V^{2+}(d^3)$, and $V^{+}(d^4)$ ions in ZnTe. It contains only ground and first excited states of these ions. The numbers represent the reactions discussed in the text and listed in Table II. Transitions represented by broken lines are not detected. The V^{2+}/V^{3+} donor level is the t_2 level in the V^{2+} column and the V^{2+}/V^{+} acceptor level is the t_2 level in the V^{+} column.

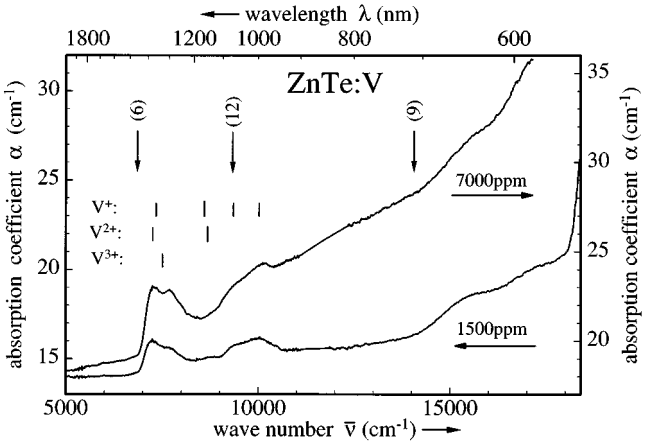

FIG. 6. Absorption spectra of ZnTe:V samples with a nominal concentration of 1500 ppm (*lower curve and left scale*) and 7000 ppm (*upper curve and right scale*) at $T=4$ K. The origin of the absorption bands of internal transitions of the respective ionization states of vanadium and the charge-transfer bands are also indicated. Decadic absorption coefficient is not corrected for reflection. Presence of V^{2+} should produce the dominant peaks at 7200 and 8700 cm^{-1}, which are barely visible.

a CT transition at about 14 000 cm^{-1}. The starting point of this CT band was determined by a fit to the $\frac{2}{3}$ power law as 13 450 cm^{-1}. This energy lies between the threshold points of the CT process (9) (14 050 cm^{-1}) and the donor process (5) (13 000 cm^{-1}).

After 9400-cm^{-1} pulse excitation, the 6000-cm^{-1} emission band decays exponentially with $\tau=(48\pm5)$ μs and the 8600-cm^{-1} band (after 18 800-cm^{-1} pulse excitation) exponentially with $\tau=(71\pm3)$ μs. The decay of the 6000 cm^{-1} emission is no more a simple exponential upon 18 800-cm^{-1} excitation, and for different parts of the time-dependent spectrum, two time constants were derived as 55 and 135 μs, approximately.

There are not yet enough facts available to decide if these two luminescence bands have a similar origin or a relationship to one of the three V oxidation states, or if some completely different center is responsible for these emissions, for example related to some of the complexes detected by electron paramagnetic resonance (EPR) (see paper II).

C. Crystal-field calculations

The optical spectra presented in the previous sections are now considered in terms of crystal-field transitions. Among various crystal-field parametrization schemes, the basic approach formulated by Tanabe and Sugano (TS) has proved to give a reasonable and coherent description of transitions between d^n multiplet levels. Other models usually need additional fitting parameters, but are not necessarily more suitable.[21] In these Tanabe-Sugano computations, the eigenvalues of Griffith matrices[22] representing the crystal-field states were fitted to the barycenters of the excitation bands.

The low-energy emission band near 3130 cm^{-1} (cf. Fig. 1) and the corresponding excitation spectrum (cf. Fig. 2) have been accounted for by internal $V^{+}(d^4)$ transitions in Sec. II B. For a reasonable tetrahedral crystal field Δ, a d^4 electron system exhibits a ${}^5T_2(D)$ ground state and a ${}^5E(D)$ excited state with lowest energy. In the Tanabe-Sugano scheme, the energy separation of these levels is identical to the crystal-field parameter Δ. Neglecting fine-structure effects, its value is directly given by the ${}^5E(D)\rightarrow{}^5T_2(D)$ transition energy. Since the corresponding excitation band has not been recorded, its barycenter is estimated by adding the energy difference between the barycenter of the emission band and its corresponding NPL to the average NPL energy. This procedure implies a symmetrical Stokes shift for absorption and emission bands.

Among the excited states above ${}^5E(D)$, only triplet levels are considered further. The excitation spectrum Fig. 2 exhibits two dominating bands peaking at 7250 and 10 000 cm^{-1}. The latter one shows a pronounced shoulder at the low-energy side and a weak broadening at the high-energy slope. The structures indicate a superposition of transitions to different crystal-field levels. A comparison of the spectrum with a Tanabe-Sugano diagram, as displayed in Fig. 7, gives straightforward assignments of the observed transitions. The intensive low-energy excitation is assigned to a transition into the lowest triplet state ${}^3T_1(H)$. Subsequently, the structures of the excitation spectrum are assigned to crystal-field levels as indicated in Fig. 2 and Table I. Within the broad band near 10 000 cm^{-1}, no structure could be attributed to a transition into the ${}^3E(H)$ state, which is believed to be obscured by close-lying stronger transitions. No structures could be connected with transitions into levels above 11 000 cm^{-1}. The excitation spectrum displays only a weak broad band here, extending up to a thresholdlike increase near 14 000 cm^{-1} studied in Sec. II D. The structureless band is believed to originate from the Tanabe-Sugano regime above the upper ${}^3T_2(F)$ state. This range exhibits a high density of crystal-field levels not resolved in the spectrum.

The assignments discussed above are strongly supported by comparable structures found in ZnS:V and ZnSe:V.[11] Some differences observed with ZnTe should, however, be

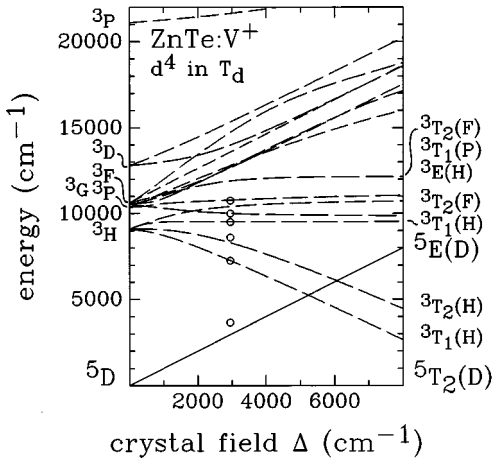

FIG. 7. Tanabe-Sugano fit for the $V^+(d^4)$ ion in ZnTe, $B=310$ cm^{-1}, $C=1960$ cm^{-1}, $\Delta=2950$ cm^{-1}. The circles represent the experimental positions of the excitation bands.

mentioned. The change of the chalcogene from S and Se to Te in the host crystal does not only induce an obvious significant decrease in the transition energies. The high ratio of $C/B=6.3$, necessary for a suitable fit in ZnTe, indicates changes in the radial distribution of the d^4 electrons. Furthermore, a chemical trend may be read from the intensities of some transitions observed in the excitation spectra of the three materials. In addition, a determination of the parameter Δ by the above-mentioned procedure does not lead to reasonable fit results for ZnTe. This indicates differences in the vibronic properties, as compared to ZnS and ZnSe.

The emission band peaking at 3580 cm^{-1} (cf. Fig. 1) and its excitation structures (cf. Fig. 3) have been attributed to the $V^{2+}(d^3)$ transitions above. To define an empirical transition energy of the lowest excited state, the same reflection procedure, as described above for the transition to the $^5E(D)$ state of V^+, was applied. The level scheme of a d^3 ion comprises both quartet and doublet levels (Fig. 8). Similar to ZnS:V^{2+} and ZnSe:V^{2+}, the ground state turns out to be the

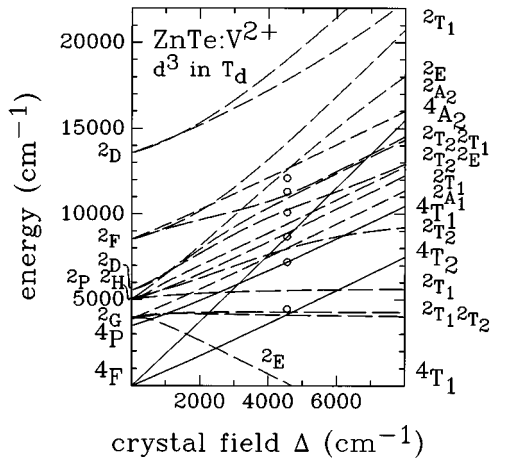

FIG. 8. Tanabe-Sugano fit for the $V^{2+}(d^3)$ ion in ZnTe, $B=232$ cm^{-1}, $C=983$ cm^{-1}, $\Delta=4548$ cm^{-1}. The circles represent the experimental positions of the excitation bands.

usual high-spin state $^4T_1(F)$. It is interesting, however, to note the close vicinity of a change over to the low-spin ground state $^2E(G)$, which is even closer here than in ZnSe:V^{2+}. The intense excitation bands centered at 7200 cm^{-1} and near 8700 cm^{-1} originate from spin-allowed transitions to the quartet states $^4T_1(P)$ and $^4A_2(F)$, respectively. All further, weaker structures arise from spin-forbidden transitions to doublet levels.

In the fitting procedure, the parameters B and Δ were defined by the quartet levels, because the corresponding matrix elements do not contain C. All weak structures are thus fitted only by the single parameter C (Fig. 8). The set of parameters resulting from the fit reflects the decrease of the transition energies by passing from ZnS:V over ZnSe:V to ZnTe:V. The decrease does not significantly affect the C/B ratio and is thus essentially described by a simple down scaling.

Crystal-field calculations with the intent of confirming the assignment to V^{3+} (d^2) of the emission band centered at 4450 cm^{-1} are less prolific. Two transitions into triplet states are expected above the resonant excitation of the luminescence. Since only one excitation band was found and no additional structures due to singlet transitions could be recognized, the parameters B and Δ were adjusted to two experimental energies in a first step. The transition energy of the resonant excitation band was again derived by the procedure described for V^+.

Despite the poor database, the calculation yields reasonable results. The evaluated B parameter (278 cm^{-1}), shows a chemical trend with an equal ratio between ZnSe/ZnS and ZnTe/ZnSe. A comparable trend is found for the calculated transition to the $^3T_1(P)$ level (near 11 800 cm^{-1}), which is not detected in the excitation (Fig. 4) nor in the absorption spectra (Fig. 6). Since crystal-field considerations cannot be regarded as unfailing confirmation, further arguments should be obtained from charge-transfer and sensitization properties of vanadium in ZnTe.

D. Sensitization spectra

The sensitization spectra of the three inner vanadium emissions (2), (3), and (4) are displayed in Figs. 9 and 10. The involved CT processes are symbolized by numbers in parentheses and the estimated starting points are indicated by vertical dashed lines. All the spectra are referred to the same zero point, the curves are not shifted in y direction, only enlarged or shrunk. Therefore, it is possible to take directly the relative stimulation or quenching of the processes from the spectra and to compare them. The dashed horizontal lines indicate the signal level without ancillary excitation. Commonly, the sensitization spectra correspond exactly to the behavior known from the excitation spectrum under additional excitation. The sensitization spectra add important information, however, concerning the onsets of the CT processes.

In Figs. 9 and 10, the choice of sensitization experiments of the three V emissions is demonstrated, with comparatively low (Fig. 9) and high (Fig. 10) energy of the primary modulated excitation. No sensitization of V^+ emission was detected under low-energy primary excitation in the $^3T_1(H)$ absorption band at 7200 cm^{-1}. The sensitization behavior of the V^+ emission was also measured at three different

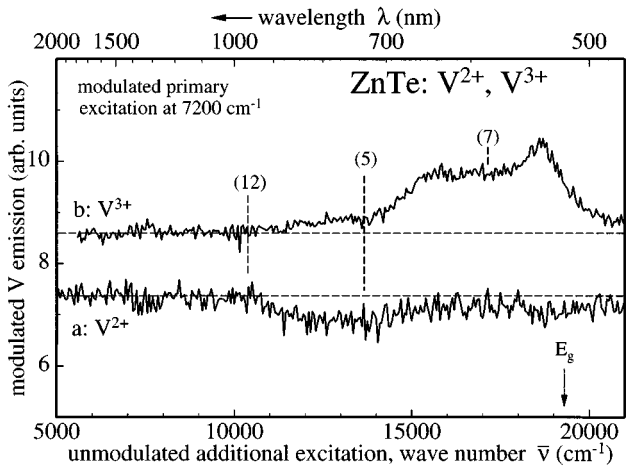

FIG. 9. Sensitization spectra of the (a) $^4T_2(F)\rightarrow{}^4T_1(F)$ luminescence of $V^{2+}(d^3)$ and (b) $^3T_2(F)\rightarrow{}^3A_2(F)$ luminescence of $V^{3+}(d^2)$ in ZnTe at $T=4.2$ K. Primary modulated excitation in the region $\overline{\nu}=6830-7560$ cm^{-1}. Detected range of the modulated emissions: (a) $\overline{\nu}=3330-3950$ cm^{-1}, (b) $\overline{\nu}=4350-4760$ cm^{-1}.

intermediate-energy primary modulated excitations. Under excitation at 10 000 cm^{-1}, i.e., in the second $^3T_1(H)$ band, the quenching is very weak ($\leqslant -5\%$) above 7000 cm^{-1}. But this situation changes considerably under the excitation at 13 300 cm^{-1} or 15 400 cm^{-1}. The shape of the curves is then similar to curve (a) in Fig. 10. The strongest relative V^+ stimulation ($\approx +25\%$) exists under 13 300 cm^{-1} primary excitation at wave numbers $\geqslant$14 000 cm^{-1}. It reflects exactly the situation in the excitation spectrum (cf. Fig. 2), because, in fact, the emission starts at the lowest signal level at this primary excitation.

The sensitization spectra of the V^{2+} emission at three medium energies of primary excitation (8300, 10 000, and 13 300 cm^{-1}) were recorded as well. The comparatively strongest stimulation ($\approx +170\%$ at 15 000 cm^{-1}) is measured in the case of 10 000 cm^{-1} primary excitation under an unmodulated additional excitation above 11 000 cm^{-1}. But one should consider that the V^{2+} emission under 10 000 cm^{-1} excitation is very weak (cf. Fig. 3). Under 8300 cm^{-1} excitation, also a stimulation exists in the same 12 000–18 000-cm^{-1} region, but just about +16%. No quenching is measured for these two (8300- and 10 000-cm^{-1}) primary excitations. The shape of the sensitization curve under 13 300-cm^{-1} primary excitation is very similar to curve (b) of Fig. 10, but the stimulation in the 12 000–18 000 cm^{-1} region is only weak ($\approx +7\%$) and an additional excitation at 8000 cm^{-1} quenches the emission only by $\approx -27\%$. All the three curves of V^{2+} display a rise at about 10 500 cm^{-1}, which can be assigned to the CT processes (11) or (12).

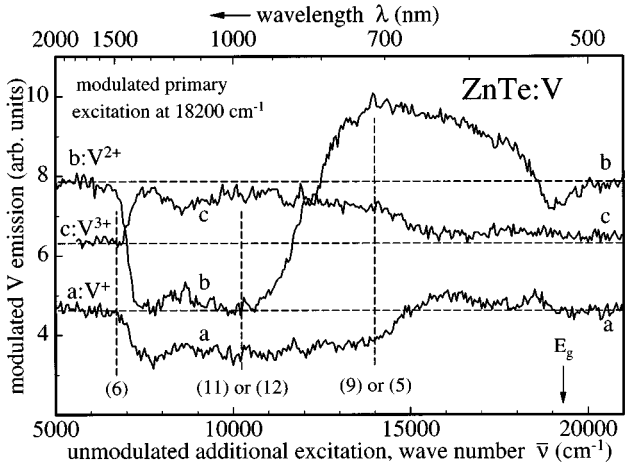

FIG. 10. Sensitization spectra of the three internal luminescence transitions of (a) $V^+(d^4)$, (b) $V^{2+}(d^3)$, and (c) $V^{3+}(d^2)$ in ZnTe at $T=4.2$ K. Primary modulated excitation was just below the gap energy at $\overline{\nu}=17\,400-19\,000$ cm^{-1}. The detected range of the modulated emissions was the same as in Figs. 2–4. The curves (a) of V^+ and (c) of V^{3+} exhibit opposite trends, while the curve (b) of V^{2+} displays a more complicated form. The excitation situation and the results at 14 000 cm^{-1} correspond to the dashed line of Fig. 1.

In Fig. 9, curve (a), however, a quenching of V^{2+} starts at this energy (10 500 cm^{-1}). Under primary excitation (7200 cm^{-1}) in the strong spin-allowed $^4T_1(P)$ band (cf. Fig. 3), the relative sensitization of the V^{2+} emission is very small (Fig. 9 curve a), as with V^+. On the contrary, the V^{3+} emission can be stimulated relatively well under this primary excitation (Fig. 9, curve b). Here, it is possible to identify the three CT processes (12), (5), and probably (7).

Figure 10 displays the sensitization spectra of the V^+ (curve a), V^{2+} (b), and V^{3+} (c) emissions under near-gap primary excitation. The sensitization spectra of V^{3+} and V^+ show exactly inverse tendencies, while the V^{2+} signal exhibits a strongly modulated curve (b). At the beginning, both the V^+ and V^{2+} emissions (curves a and b, respectively) are diminished by process (6), but at 10 500 cm^{-1}, the curve (b) rises steeply. At 14 000 cm^{-1} (process 9 or 5), the rise is stopped and the signal declines. This change of trend at 14 000 cm^{-1} exists also, but not as strong, in the curves (a) and (c) for V^+ and V^{3+}, respectively. While by process (6) at 6800 cm^{-1} holes are produced in the VB, in the other CT processes with opposite trends, electrons are probably lifted to the CB (see discussion). The situation for a 14 000-cm^{-1} supplementary excitation (given by the abscissa in Fig. 10), where the V^{2+} and V^{3+} emissions are stimulated while V^+ is quenched, corresponds exactly to the dashed line in Fig. 1. This correspondence demonstrates well the compatibility of the different optical methods.

III. DISCUSSION

The optical properties of vanadium in ZnTe presented in the previous section exhibit pronounced similarities to ZnS:V and ZnSe:V in the low-energy region. The resulting plausible assignments of the three luminescence bands to internal transitions of the three different oxidation states of V are supported by numerous details found in the fine structure of emission and corresponding excitation spectra. For the emission band assigned to V^{3+}, the main features are the familiar characteristic TO satellite and the fairly large time constant, which is in accordance with the assumed symmetry-forbidden transition. For the two other emission bands assigned to V^{2+} and V^+, the comparison with ZnS and ZnSe reveals a chemical trend in the vibronic coupling. The stronger phonon coupling and the softer lattice vibrational

modes in ZnTe result in less pronounced no phonon structures. Such a chemical trend on going from ZnS to ZnSe and ZnTe is also observed with respect to transition energies in the emission and excitation spectra and crystal-field parameters. Furthermore, the excitation spectra of the three emission bands show obvious similar features to the corresponding excitation bands in ZnS:V and ZnSe:V.

In the high-energy (charge-transfer) region, however, significant differences to ZnS and ZnSe are found. The different behavior in this range indicates that the deep levels of vanadium in ZnTe lie at different positions with respect to VB and CB.

The three internal V emissions are not strongly affected by additional illumination during low-energy primary excitation. Under high-energy primary excitation, the sensitization is more efficient, but it is more complicated to estimate which of the possible CT processes are actually involved.

The important CT band near 14 000 cm^{-1} in the excitation spectrum of V^+ (Fig. 2) is assigned to process (9), as in ZnSe. The threshold energy of process (9) at 14 050 cm^{-1} derived from the excitation spectrum of V^+ matches well the energy of process (12) and the gap energy of ZnTe (see Fig. 5 and Table II). According to this model, the equation

$$E_g - E_{(12)} + E_{(3)} = E_{(9)}$$

is valid. The experimental values $19\,300 - 9400 + 4056 \cong 14\,000$ cm^{-1} are in good agreement with this conception. The data provide experimental evidence, that the energy spacing between the t_2 and e levels of V^+ (right column in Fig. 5) is equal to the energy of process (3) in the one-electron model [note that the process (3) is the internal V^{2+} transition].

The approximations of the CT band (6) in the excitation spectrum of V^{3+} (Fig. 4) following the method of Ref. 19 prove, that the V^{3+} ion is a center with heavy-hole character. Process (6) in the excitation spectrum of $V^{3+}(d^2)$ and in the sensitization experiments of Fig. 10 determines the V^{3+}/V^{2+} donor level at 6800 cm^{-1} above the VB, i.e., V^{2+}/V^{3+} lies 12 500 cm^{-1} below the CB. Process (12) in the excitation spectrum of V^{2+} (Fig. 3) determines the V^{2+}/V^+ acceptor level at 9400 cm^{-1} above the VB. From the given positions of the donor and acceptor levels, the Hubbard energy of vanadium can be obtained as $9400-6800$ $cm^{-1} = 2600$ cm^{-1}. Irrespective of future more detailed deliberations concerning trends in II-VI materials, it is to be stated here, that this value is definitely smaller than previous estimations for ZnS and ZnSe.

It should be noted that the present model does not require the participation of summation or difference processes as supposed in the interpretation of, e.g., ZnSe:Ti spectra.[10] This is remarkable insofar as our recent experiments on V impurities in ZnS and ZnSe point towards an interplay of these more complicated possibilities.

Although the presented interpretations of the optical properties of V in ZnTe and the EPR results discussed in the accompanying paper (Kreissl *et al.*) provide a coherent description, there are still some open questions which can hopefully become the subject of further optical studies. Concerning the connection of PL and EPR, a clear correlation of the V complexes detectable in EPR to features in the optical spectra and the detection of V^+ found in PL to resonance's in EPR is missing yet. In the optical spectra, a fine structure related to the (V^+,e^+) complex assumed to be active in the excitation spectrum of $V^{2+}(d^3)$ should be detectable. Finally, the absorption spectrum is somewhat puzzling, since V^{2+} features are barely visible, while V^+ and V^{3+} are detectable. Here, the ${}^3T_1(F)$ transition of V^{3+} corresponds to a dip in the absorption curve of Fig. 6, so that a reabsorption process is conceivable.

To conclude, the results of the present study depict a description of the vanadium impurity in various charge states and their transformations. Although the measurements have almost exclusively been performed at low temperatures, where the characteristic properties become more clearly observable, the consequences for room-temperature behavior would enable future studies, also aimed at potential applications.

ACKNOWLEDGMENTS

It is a pleasure to thank Dr. E. E. Vogel, Temuco, Chile for some stimulating discussions. One of the authors, P.P., acknowledges the support of the Max-Planck-Gesellschaft. This paper was partially supported by the DAAD, Bonn.

*Present address: Department of Physics, University of Notre Dame, Notre Dame, IN 46556.

[1] M. Ziari, W. H. Steier, P. M. Ranon, S. Trivedi, and M. B. Klein, Appl. Phys. Lett. **60**, 1052 (1992).

[2] T. L. Larsen, C. F. Varatto, and D. A. Stevenson, J. Appl. Phys. **43**, 172 (1972).

[3] R. B. Bylsma, P. M. Bridenbaugh, D. H. Olson, and A. M. Glass, Appl. Phys. Lett. **51**, 889 (1987).

[4] A. Partovi, J. Millerd, E. M. Garmire, M. Ziari, W. H. Steier, S. B. Trivedi, and M. B. Klein, Appl. Phys. Lett. **57**, 846 (1990).

[5] P. Peka, M. U. Lehr, H.-J. Schulz, R. Schwarz, and K. W. Benz, Appl. Phys. A **58**, 447 (1994).

[6] P. Peka, M. U. Lehr, J. Dziesiaty, S. Müller, J. Kreissl, P. Rudolph, and H.-J. Schulz, Mater. Sci. Forum **143-147**, 435 (1994).

[7] G. Goetz, U. W. Pohl, and H.-J. Schulz, J. Phys. Condens. Matter **4**, 8253 (1992).

[8] S. W. Biernacki, G. Roussos, and H.-J. Schulz, J. Phys. C **21**, 5615 (1988).

[9] J. M. Langer, C. Delerue, M. Lannoo, and H. Heinrich, Phys. Rev. B **38**, 7723 (1988).

[10] J. Dziesiaty, P. Peka, M. U. Lehr, H.-J. Schulz, and A. Klimakow, Phys. Rev. B **49**, 17 011 (1994).

[11] G. Goetz, U. W. Pohl, H.-J. Schulz, and M. Thiede, J. Lumin. **60/61**, 16 (1994).

[12] E. E. Vogel (private communication).

[13] U. Kaufmann, H. Ennen, J. Schneider, R. Wörner, J. Weber, and F. Köhl, Phys. Rev. B **25**, 5598 (1982).

[14] V. S. Vavilov, V. V. Ushakov, and A. A. Gippius, Physica **117B & 118B**, 191 (1983).

[15] V. I. Sokolov, Fiz. Tverd. Tela (Leningrad) **29**, 1848 (1987) [Sov. Phys. Solid State **29**, 1061 (1987)].

[16] M. J. Kane, M. S. Skolnick, P. J. Dean, W. Hayes, B. Cockayne, and W. R. MacEwan, J. Phys. C **17**, 6455 (1984).

[17] N. Vagelatos, D. Wehe, and J. S. King, J. Chem. Phys. **60**, 3613 (1974).
[18] S. G. Bishop, D. J. Robbins, and P. J. Dean, Solid State Commun. **33**, 119 (1980).
[19] V. I. Perel' and I. N. Yassievich, Zh. Eksp. Teor. Fiz. **82**, 237 (1982) [Sov. Phys. JETP **55**, 143 (1982)].
[20] G. Nimtz, in *Semiconductors: Physics of II-VI and I-VII Compounds, Semimagnetic Semiconductors*, edited by O. Madelung, Landolt-Börnstein, New Series, Group III, Vol. 17, Pt. b (Springer, Berlin, 1982).
[21] K. Klein, J. Dreyhsig, H.-E. Gumlich, M. Thiede, G. Goetz, H.-J. Schulz, and J. W. Allen, Phys. Status Solidi A **130**, K207 (1992).
[22] J. S. Griffith, *The Theory of Transition Metal Ions*, 3rd ed. (Cambridge University Press, Cambridge, England, 1971).